Combustion Theory and Modelling
Publication details, including instructions for authors and subscription information:
http://www.tandfonline.com/loi/tctm20

Turbulent piloted partially-premixed flames with varying levels of O_2/N_2: stability limits and PDF calculations

Mrinal Juddoo [a], Assaad R. Masri [a] & Stephen B. Pope [b]
[a] School of Aerospace, Mechanical and Mechatronic Engineering, The University of Sydney, NSW, 2006, Australia
[b] Mechanical and Aerospace Engineering, Cornell University, Ithaca, NY, 14853, USA

Available online: 23 May 2011

To cite this article: Mrinal Juddoo, Assaad R. Masri & Stephen B. Pope (2011): Turbulent piloted partially-premixed flames with varying levels of O_2/N_2: stability limits and PDF calculations, Combustion Theory and Modelling, 15:6, 773-793

To link to this article: http://dx.doi.org/10.1080/13647830.2011.563867

Combustion Theory and Modelling
Vol. 15, No. 6, 2011, 773–793

Turbulent piloted partially-premixed flames with varying levels of O_2/N_2: stability limits and PDF calculations

Mrinal Juddoo[a]*, Assaad R. Masri[a] and Stephen B. Pope[b]

[a]*School of Aerospace, Mechanical and Mechatronic Engineering, The University of Sydney, NSW 2006, Australia;* [b]*Mechanical and Aerospace Engineering, Cornell University, Ithaca, NY 14853, USA*

(*Received 4 November 2010; final version received 6 February 2011*)

This paper reports measured stability limits and PDF calculations of piloted, turbulent flames of compressed natural gas (CNG) partially-premixed with either pure oxygen, or with varying levels of O_2/N_2. Stability limits are presented for flames of CNG fuel premixed with up to 20% oxygen as well as CNG–O_2–N_2 fuel where the O_2 content is varied from 8 to 22% by volume. Calculations are presented for (i) Sydney flame B [Masri et al. 1988] which uses pure CNG as well as flames B15 to B25 where the CNG is partially-premixed with 15–25% oxygen by volume, respectively and (ii) Sandia methane–air (1:3 by volume) flame E [Barlow et al. 2005] as well as new flames E15 and E25 that are partially-premixed with 'reconstituted air' where the O_2 content in nitrogen is 15 and 25% by volume, respectively. The calculations solve a transported PDF of composition using a particle-based Monte Carlo method and employ the EMST mixing model as well as detailed chemical kinetics. The addition of oxygen to the fuel increases stability, shortens the flames, broadens the reaction zone, and shifts the stoichiometric mixture fraction towards the inner side of the jet. It is found that for pure CNG flames where the reaction zone is narrow ($\sim$0.1 in mixture fraction space), the PDF calculations fail to reproduce the correct level of local extinction on approach to blow-off. A broadening in the reaction zone up to about 0.25 in mixture fraction space is needed for the PDF/EMST approach to be able to capture these finite-rate chemistry effects. It is also found that for the same level of partial premixing, increasing the O_2/N_2 ratio increases the maximum levels of CO and NO but shifts the peak to richer mixture fractions. Over the range of oxygenation investigated here, stability limits have shown to improve almost linearly with increasing oxygen levels in the fuel and with increasing the contribution of release rate from the pilot.

Keywords: piloted flames; partially-premixed; PDF calculations; local extinction; re-ignition

1. Introduction

Capabilities to compute the finite-rate chemistry effects in turbulent non-premixed flames have improved significantly with advanced approaches such as transported probability density function methods (PDF) [1], conditional moment closure (CMC) [2,3], multiple mapping closure (MMC) [4] and the multi-variable laminar flamelet methods where the mixture fraction, scalar dissipation rates and transient time scales are used as independent variables [5,6]. More recently, the mixture fraction and reaction progress variable concepts

*Corresponding author. Email: mrinal.juddoo@sydney.edu.au

ISSN: 1364-7830 print / 1741-3559 online

http://dx.doi.org/10.1080/13647830.2011.563867
http://www.tandfonline.com

were merged [7–9] to enable computation of partially premixed flames. While all of these approaches perform well in computing finite-rate chemistry effects for fuel mixtures where the reaction zones are broad, they tend to be less successful in flows where the reaction zones become narrower as is the case for pure CNG or methane flames. While the reasons for such deficiencies differ depending on the method, the challenge to modellers extends beyond the scope of non-premixed flames. The demand is for a universal computational approach capable of accounting for finite-rate chemistry effects in the entire turbulent combustion regime extending from non-premixed to premixed flames. Such developments will facilitate the transition towards computing more complex processes such as soot formation and the combustion of sprays.

Turbulent premixed, stratified as well as partially-premixed flames are now receiving considerable attention with attempts to mirror the advances achieved in the non-premixed domain [10–12]. In premixed combustion, the piloted jet burner in hot vitiated co-flows is gradually established as a model problem for studying finite-rate chemistry in highly sheared premixed flames. The reaction zones in these flows are broad and distributed [13] and the extensive data bank already available for validation points to some significant modelling challenges: The reactive/diffusive balance that prevails in normal laminar premixed flames and forms the basis of the laminar flame speed concept may be undermined here and hence may be substituted by concepts where reactive/convective balances prevail. If true, this will impact on the ability of flamelet-based approaches to model such flows. With stratified combustion, various designs for generic laboratory burners are being developed [14,15] but the available data are still rather limited. While the concept of stratification applies over the entire mixture fraction range, it is mostly relevant for lean mixtures to extend the range of operation of homogeneous charge compression ignition engines [16,17]. More generally, partially-premixed combustion covers a much broader regime of mixture fractions and, while common in many practical applications, remains less understood and more difficult to compute because it straddles the complexities of both premixed and diffusion flames. The extensive database for the piloted, partially premixed flames of Barlow and Frank [18] forms an excellent platform for extending knowledge to a broader range of mixture fractions.

The piloted burner configuration is adopted here to study partially-premixed flames where pure oxygen or varying ratios of O_2/N_2 are partially-premixed with compressed natural gas (CNG). Increasing levels of oxygen in the fuel broadens the reaction zone and increases the stoichiometric mixture fraction, ξ_s but impacts the compositional structure of turbulent flames in ways that are not well understood [19]. The limit of combustion in pure oxygen is particularly attractive for stationary power generation as it facilitates carbon-sequestration [20,21]. In this paper, the level of oxygen was increased from 0 to 25% in pure CNG flames approaching extinction (variations on Sydney flames L, B, M) and different O_2/N_2 ratios were added to CNG–O_2–N_2 flames while keeping the overall stoichiometry unchanged (variations on Sandia flames D, E, F). The measured stability characteristics are presented and a series of flames with different CNG–O_2–N_2 mixtures were selected for calculations using a transported composition PDF approach with detailed chemistry. The limitations of the PDF approach are discussed along with the effects of oxygenation on the computed structure of the flames.

2. Measurement of stability limits

The piloted burner used here is identical to the one used in earlier studies of CNG [22] and methane–air flames [18, 23]. This is intentional considering the wealth of knowledge and

data already available for these flames. The burner has a central fuel jet 7.2 mm in diameter and an annular pilot with a diameter of 18.9 mm with the entire assembly centred in a co-flowing air stream. The pilot is composed of a mixture of acetylene hydrogen and air with the same nominal enthalpy and equilibrium composition as a methane/air flame at the same stoichiometry. For a given fuel mixture, the key controlling parameters are central jet velocity, the heat release from the pilot which may be varied by varying the stoichiometry or the velocity of the fuel/air mixture through the pilot stream or both. The velocity in the pilot stream is expressed in terms of the burnt pilot velocity, u_{pb} which is given by the product of the bulk velocity of the unburnt pilot mixture, u_{pu} in the annulus times the *unburnt*/*burnt* density ratio. For a stoichiometric pilot with a peak temperature of about 2400K (accounting for some radiation losses), the ratio is around eight so that u_{pb}–$8u_{\mathrm{pu}}$. CNG (with a volumetric composition of 88.8% CH_4, 7.8% C_2H_4, 1.9% CO_2, 1.2% N_2 with the remaining 0.3% being a mixture of propane, propene, butane and pentanes) is used here as a parent fuel instead of pure methane and blow-off experiments to determine the stability limits are conducted for the two following sets of fuel configurations:

(1) The CNG fuel is partially-premixed with an increasing amount of oxygen, ranging from 5 to 25% by volume and the blow-off limits are determined for different burnt pilot velocities, u_{pb}. For consistency, an identical definition for blow-off is used as in earlier experiments [22]. It is the condition before which the flame is still connected to the burner but hardly visible further downstream giving a faint rumbling noise. The fuel jet blow-off velocity u_{BO}, is determined for pilot velocities $u_{\mathrm{pb}} = 12$, 16, 20, and 24 m/s for all fuel mixtures, as shown on Table 1. The fuel/air mixture in the pilot is kept at stoichiometric conditions throughout these experiments and the co-flow air velocity is fixed at 15 m/s.
(2) The CNG fuel is partially-premixed with an O_2+N_2 mixture, referred here as 'reconstituted air', which has varying volume fractions of oxygen in nitrogen. Air, initially with 21% oxygen and 79% nitrogen, is 'reconstituted' such that the $[O_2/(O_2+N_2)]$ ratio is varied from 21% down to 10% and up to 30%, while the stoichiometric mixture fraction of the fuel mixture is maintained at $\xi_{\mathrm{s}} = 0.35$. These flames differ from the pure CNG and CNG–O_2 flames in three aspects: (i) the co-flow air velocity is 0.9 m/s instead of 15 m/s, (ii) the pilot composition is equivalent to the products of a methane/air flame at an equivalence ratio of 0.77 instead of stoichiometric conditions so that the temperature in the pilot stream is 1880 K, and (iii) the bulk velocity in the pilot stream, u_{pb}, is varied such that the heat release from the pilot is kept at either 4, 6, 8, or 10% of the main jet's heat release, as shown in Table 1.

The flammability limits of methane have been investigated from previous studies [24] and shown on Figure 1 with reference to the chosen fuel mixtures described in Table 1. It can be seen that all mixtures are far away enough from the upper flammability limit of methane in oxygen and nitrogen, and consequently behave as diffusion flames, despite the partial-premixture of the fuel with the oxidizer.

2.1. *Reaction zone width in mixture fraction space, $\Delta\xi_R$*

The reaction zone width, $\Delta\xi_{\mathrm{R}}$ is calculated in mixture fraction space from laminar simulations of counter-flow diffusion flames of the various fuel mixtures selected. A lean reactive limit, ξ_{Lean} and a rich reactive limit, ξ_{Rich} are defined as the points at which the

Table 1. Relevant parameters for the investigated fuels.

	Main jet				Pilot			
	Composition (mole fraction)			Stoich. mixt. fraction	Equiv. ratio	Burnt velocity	Heat release contribution	Coflow Air velocity
Fuel type	CNG	O_2	N_2	ξ_s	φ	u_{pb} (m/s)	%	$u_e(m/s)$
CNG	1.00	0.00	0	0.055	1.0	12, 16, 20, 24		15
CNG–O_2	0.95	0.05	0	0.062	1.0	12, 16, 20, 24	Decreases with increasing jet velocity	15
CNG–O_2	0.90	0.10	0	0.070	1.0	12, 16, 20, 24		15
CNG–O_2	0.85	0.15	0	0.080	1.0	12, 16, 20, 24		15
CNG–O_2	0.80	0.20	0	0.091	1.0	12, 16, 20, 24		15
CNG–O_2–N_2	0.21	0.08	0.71	0.351	0.77		4, 6, 8, 10	0.9
CNG–O_2–N_2	0.23	0.12	0.65	0.351	0.77		4, 6, 8, 10	0.9
CNG–O_2–N_2	0.25	0.16	0.59	0.351	0.77	Increases with increasing jet velocity	4, 6, 8, 10	0.9
CNG–O_2–N_2	0.26	0.18	0.55	0.351	0.77		4, 6, 8, 10	0.9
CNG–O_2–N_2	0.28	0.22	0.50	0.351	0.77		4, 6, 8, 10	0.9

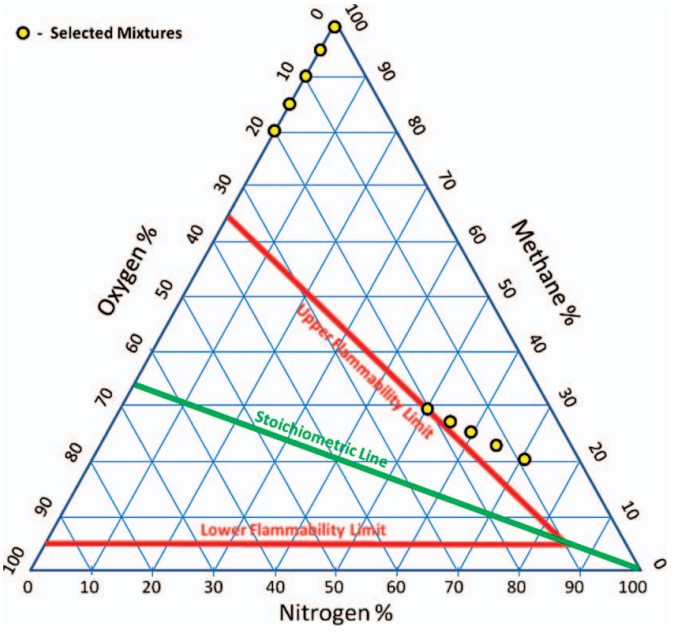

Figure 1. Flammability limits of methane–oxygen–nitrogen mixtures. Filled circles represent the selected fuel mixtures for further investigation.

net production rates of major species such as CH_4, CH_3OH, CO_2, CO, O_2, OH, H_2, and H_2O fall to below 10% of their peak value, on the lean and rich sides of stoichiometry, respectively. The reaction zone width is then calculated as being the difference between the two reactive limits, $\Delta\xi_R = \xi_{Rich} - \xi_{Lean}$. The laminar flame calculations were carried out for all fuel mixtures and their respective extinction strain rate was determined. A series of low, intermediate and high strain rate calculations, corresponding to 10, 50, and 90% of the extinction rate, were then carried out for each fuel mixture and the results averaged to obtain the reaction zone width.

A complete description of the calculation method can be found in [25]. It is worth noting that increasing the oxygen content in the jet from 0 to 25% only doubles the stoichiometric mixture fraction from $\xi_s = 0.055$ to 0.104 but increases the reaction zone width in mixture fraction space by almost three times, from $\Delta\xi_R = 0.108$ to 0.306.

2.2. *Results of blow-off experiments*

Figure 2 shows the jet blow-off velocity, u_{BO} for a range of CNG–O_2 fuels plotted vs. different values of the pilot burnt velocity, $u_{pb} = 12$, 16, 20 and 24 m/s with a co-flowing air velocity of 15 m/s. It is evident that, for the range of flames investigated, the stability limit improves almost linearly with increasing oxygen content (as well as with increasing u_{pb}). The pure CNG flames, L, B, M studied earlier are shown on the plot (at zero percent oxygen and $u_{pb} = 24$ m/s) and these are at 60, 70, and 80% of the blow-off velocity ($u_{BO} =$ 68 m/s). Figure 3 shows the blow-off velocities for a range of CNG–O_2–N_2 fuel mixtures plotted vs. the percentage of heat release from the pilot which is changed by increasing the bulk velocity while keeping the overall equivalence ratio at $\varphi = 0.77$. The co-flow air

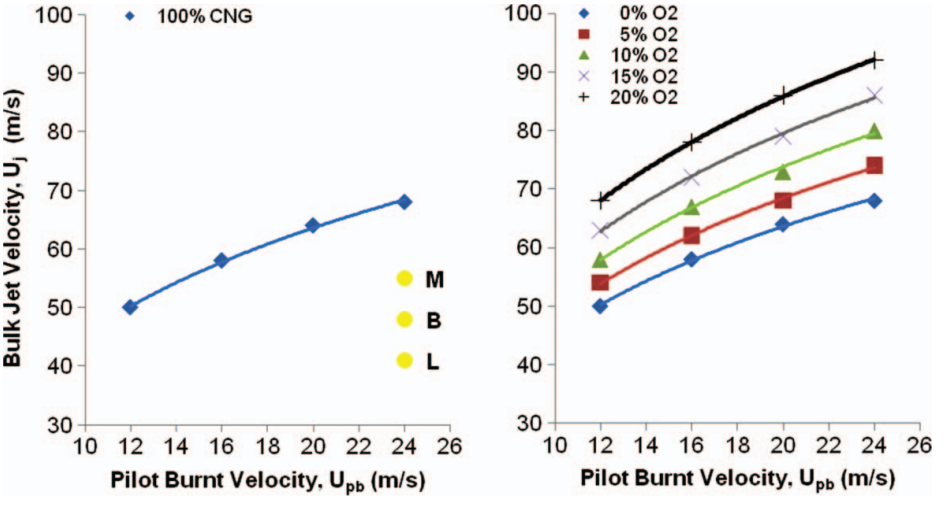

Figure 2. Blow-off limits showing the bulk jet velocity at blow-off, u_{BO} for pure CNG flames as well as for various CNG–O_2 mixtures plotted vs. the pilot burnt gas velocity, u_{pb}. Flames L, B, and M (filled circles) are shown at $u_{pb} = 24$ m/s with respect to the blow-off limit of pure CNG flames.

velocity in this case is kept at 0.9 m/s. Sandia flames D, E, and F which use CNG–air and 6% heat release from the pilot are also shown on Figure 3 with reference to the blow-off limits corresponding to 21% oxygen in nitrogen.

There is a consistent improvement in the stability limits as the level of oxygen in the fuel mixture increases. Over the range of flames examined, the blow-off velocities, u_{BO}, increase almost linearly with the oxygen concentration. Increased heat release from the

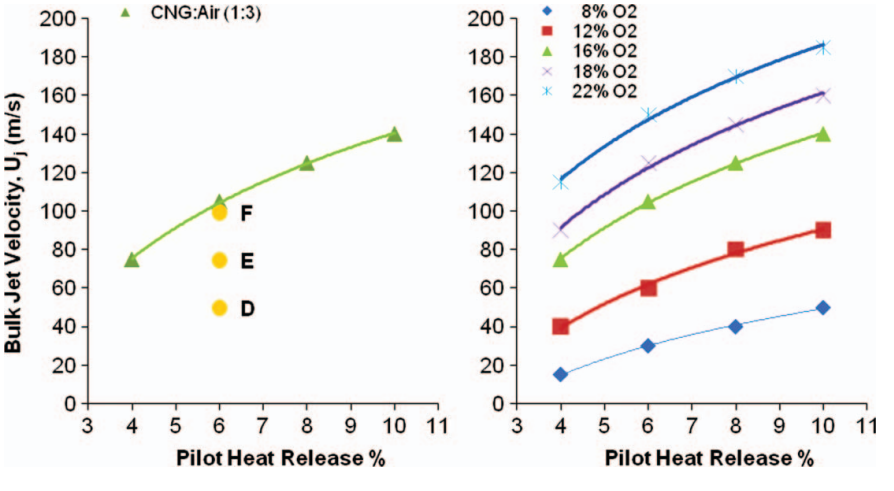

Figure 3. Blow-off limits showing the bulk jet velocity at blow-off, u_{BO} for pure CNG–air (1:3 by volume) flames as well as for various CNG–O_2–N_2 mixtures ($\xi_s = 0.35$) plotted vs. the percentage contribution to heat release from the pilot towards that of the main jet. Flames D, E, and E (filled circles) are shown with respect to the blow-off limit of CNG–air (16% O_2 by volume) flames with 6% heat release contribution from the pilot.

pilot leads to more stable flames, and higher blow-off limits due to a 'firmer' anchorage at the base of the flame at the jet exit. Close the blow-off, the flames become sensitive to the pilot heat release rate, and a minor increase in the pilot velocity can change a flame from being intermittent to fully-connected and stably burning. It should be noted that increasing the levels of oxygen premixing with CNG beyond the levels reported here would reach the flammability limit of the fuel and hence result in a premixed flame. This paper focuses on partially-premixed flames and hence the level of oxygen in the fuel mixture is intentionally kept above the flammability limit.

2.3. *Selected flames for further investigation*

A series of flame cases are selected here to study the effects varying the oxygen content in a baseline fuel mixture. Starting with pure methane flames (referred to as reference flames L, B, or M), increasing the oxygen content in the fuel increases the stoichiometric mixture fraction but the flames are maintained at the same departure from blow-off as the reference flame. For Sandia's reference flames (D, E, or F), the oxygen content in the CNG–O_2–N_2 mixture is varied while keeping both the stoichiometric fraction as well as the departure from blow-off unchanged. This paper addresses only flames B and B5–B25, referred to as 'Series B' flames, the characteristics of which are presented in Table 2. Flames B5 to B25 refer, respectively, to oxygen content of 5–25% by volume in CNG with all the flames being at 70% of the blow-off jet velocity (as is the case for flame B). All flames in 'Series B' have a pilot at stoichiometric conditions and a co-flow velocity of 15 m/s. Similarly, and with reference to Sandia flames D, E, and F, this paper deals only with flames E (also labelled E21 here), E15 and E25, referred to as 'Series E' flames. The characteristics of these flames are also shown in Table 2 and flames E15 and E25 refer to partial-premixing with 'reconstituted air' in which the $[O_2/(O_2+N_2)]$ ratio is 15 and 25%, respectively, while maintaining a fixed value of $\xi_s = 0.351$. It should also be noted that the contribution from the pilot to the total heat release of flames E15 and E25 is fixed at around 6%, as for flame E. Also, both flames E15 and E25 are at 70% of the blow-off jet velocity (as is the case for flame E). All flames in 'Series E' have a lean pilot ($\varphi = 0.77$) and a co-flow velocity of 0.9 m/s.

3. Numerical calculations

The effect of oxygenation is investigated using both laminar and turbulent flame simulations, carried out for some fuel mixtures and flames shown on Table 2. The results for some representative laminar and turbulent flame calculations are presented in this section.

3.1. *Laminar flame calculations*

Laminar flame calculations of an opposed flow diffusion flame using the open source code Cantera [26] were carried out to investigate the effect of oxygen on the structure of a series of CH_4–O_2–N_2 flames. The calculations were performed using the GRI3.0 reaction mechanism and mixture-averaged transport properties with a nominal strain rate of 60 s^{-1}. The fuel jet was set to the same composition as those described in Table 2 while the oxidiser jet was set as air throughout all laminar calculations. Results presented in Figure 4 show an increase in temperature as well as OH, NO, and CO mass fractions, with increasing oxygen content. The increase in temperature and OH is due to the lower nitrogen content of the main fuel and the broader reaction zones due to the increased oxygen levels, respectively.

Table 2. Relevant parameters for flames selected for further investigation.

		Main jet						Pilot			
			Composition (mole fraction)								
Fuel series	Fuel ref. code	Bulk jet vel. u_j (m/s)	CH_4	O_2	N_2	ξ_s	$\Delta\xi_R$	Burnt vel. u_{pb} (m/s)	Temp. (K)	Heat release %	PDF Re-ignition captured?
Series B	B	48.0	1.00	0.00	0	0.055	0.108	24	2500	~3.7	No
	B5	52.2	0.95	0.05	0	0.062	0.129	24	2500	~3.6	No
	B10	56.5	0.90	0.10	0	0.070	0.155	24	2500	~3.5	No
	B15	60.7	0.85	0.15	0	0.080	0.190	24	2500	~3.4	No
	B20	65.0	0.80	0.20	0	0.091	0.238	24	2500	~3.4	Partially
	B25	69.2	0.75	0.25	0	0.104	0.316	24	2500	~3.4	Yes
Series E	E15	42.8	0.23	0.12	0.65	0.351	0.401	9.0	1880	~6.5	Yes
	E/E21	74.4	0.25	0.16	0.59	0.351	0.503	17.1	1880	~6.5	Yes
	E25	89.1	0.26	0.18	0.55	0.351	0.588	21.3	1880	~6.5	Yes

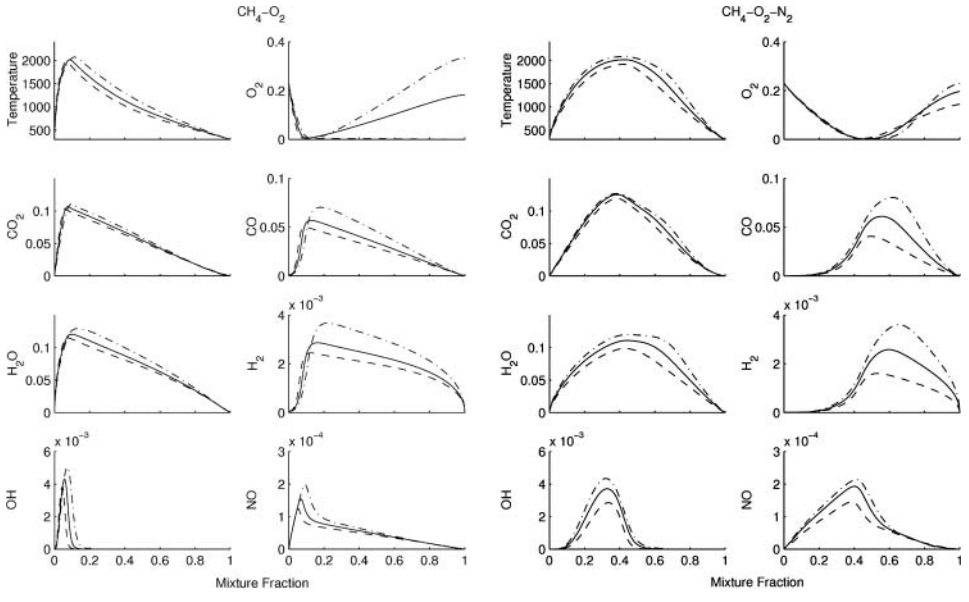

Figure 4. Laminar flame results of temperature and species mass fractions vs. mixture fraction. Left (CH_4–O_2 flames): 0% O_2 (dashed line); 10% O_2 (solid line); 20% O_2 (dash dot); Right (CH_4–O_2–N_2 flames): 12% O_2 (dashed line); 16% O_2 (solid line); 18% O_2 (dash dot) by volume.

Despite the reduction in nitrogen in the fuel, the level of NO still increases, mainly due to the higher flame temperatures enhancing the thermal-NO mechanism. CO levels also show an increase while CO_2 on the other hand, barely seems to change with only a very small increase as the oxygen levels increase. Carrying out a sensitivity analysis may shed some light in investigating this behaviour, but has not been attempted in this work. It must also be noted that radiation was included in all laminar flame calculations.

3.2. *Turbulent flame calculations*

Calculations presented here use the *FLUENT*® *6.3.26* package which solves Reynolds Averaged Navier Stokes (RANS) equations for the mean conservation of mass, momentum and energy, together with the k–ε turbulence model equations. Calculations were performed with constants $C_{\varepsilon 1} = 1.44$ and $C_{\varepsilon 2} = 1.8$ since these are deemed to yield the appropriate rate of dissipation and spreading rate for circular jets. A transport equation for the composition PDF is coupled and solved using the Lagrangian particle-based Monte Carlo method in *FLUENT*®. The ARM2 (augmented reduced mechanism) chemical kinetic mechanism [27] with 19 species including NO is employed in the calculation using the In-Situ-Adaptive Tabulation (ISAT) method [28] with an error tolerance of 1×10^{-6}. The adequacy of this tolerance level has been demonstrated in previous studies for similar flame configuration [29].

The Euclidean Minimum Spanning Tree (EMST) [30] mixing model was used with a mixing constant $C_{\varphi} = 1.5$. This value was demonstrated in previous studies to be most adequate for accounting for finite-rate chemistry effects in non-premixed jet flames [31]. The computational domain consists of 5184 mesh cells and extends 100 jet diameters axially and 50 jet diameters radially. One hundred particles per cell were used throughout

the calculations. These conditions are adopted based on earlier studies [29, 31] of numerical and modelling accuracy where issues of grid independence, boundary conditions, sensitivity to the number of particles per cell and modelling constants were optimised.

Results are presented as scatter plots of temperature and the mass fraction of selected species vs. mixture fraction, and reported in two sections. Flames in 'Series E' are the subject of the first section which discusses the impact of changing the oxygen level on the compositional structure with a particular focus on NO and CO. The second section presents results for flames in 'Series B' and discusses the limitations of the PDF/EMST approach with respect to reaction zone width in mixture fraction space. All the flames analysed are at 70% of their global blow-off limit.

3.3. *Model validation*

Figure 5 shows scatter plots of the measured temperature and species mass fractions for flame E as obtained from the Sandia's TNF web site [32] compared to the results of the numerical simulation, at various x/D locations. These comparisons confirm earlier findings that the calculations agree very well with the measurements and are able to reproduce the intensity and trends of local extinction observed experimentally as these flames approach blow-off. The ARM2 mechanism based on the GRI2.11 [33] mechanism has been shown by Cao and Pope [34] to correctly predict NO levels at upstream locations of flame E with a slight over-prediction further downstream at x/D $>$ 30. The calculations of Cao and Pope [34] included radiation effects as opposed to the ones presented in the current study and consequently, the only shortcoming in the present calculations lies in the over-prediction of NO as the overall temperature increases at x/D $=$ 30. In the work of Cao and Pope [34], it was also determined that for methane/air flames with bulk jet velocities higher than 75 m/s, the ARM2 mechanism resulted in a decrease in burning-index (BI) for temperature and species such as CO_2, H_2O, CO, OH, and H_2. An extinguished flame is obtained close to 100 m/s such as in flame F unless the pilot temperature is increased. Since flame E25 in the current study has a jet velocity of 89.1 m/s, all the calculations were carried out without radiation so as to keep boundary conditions similar in all cases without having to alter the pilot temperatures. Further calculations will be carried out at a later stage to include radiation.

Conditional means of temperature, CO, CO_2, OH, H_2O, and NO on mixture fraction are presented for flame E at x/D $=$ 15 and 30 in Figures 6 and 7, respectively. The conditional averages have been calculated using a mixture fraction bin size of 0.02 (50 bins in total). At x/D $=$ 15, the simulation results show fairly good agreement with the experiment for temperature, H_2O and CO_2 mass fractions while a slight over-prediction is observed for species such as CO, OH, and NO at the peak flame temperatures.

Downstream in the flame, at x/D $=$ 30, the temperature shows an inflexion around $\xi =$ 0.6 and similar observations are made for all species mass fractions as well. A similar effect was observed in the work of Xu and Pope [31] where a C_φ of 1.5 resulted in an inflexion in the temperature and species profiles of flames far from extinction such as flame D while a value of $C_\varphi = 2.0$ showed better agreement with experimental results. Nevertheless, as the flame approaches global extinction, the situation is reversed whereby a value of $C_\varphi = 1.5$ shows better agreement with experiment compared to 2.0. Since the current study focuses on flames approaching global blow-off, a value of $C_\varphi = 1.5$ is still deemed to be the most appropriate value to adopt throughout the calculations. Fairly good agreement is observed between the experimental and numerical results except for the over-prediction of NO which is believed to be due to the higher flame temperatures as a result of neglecting radiation.

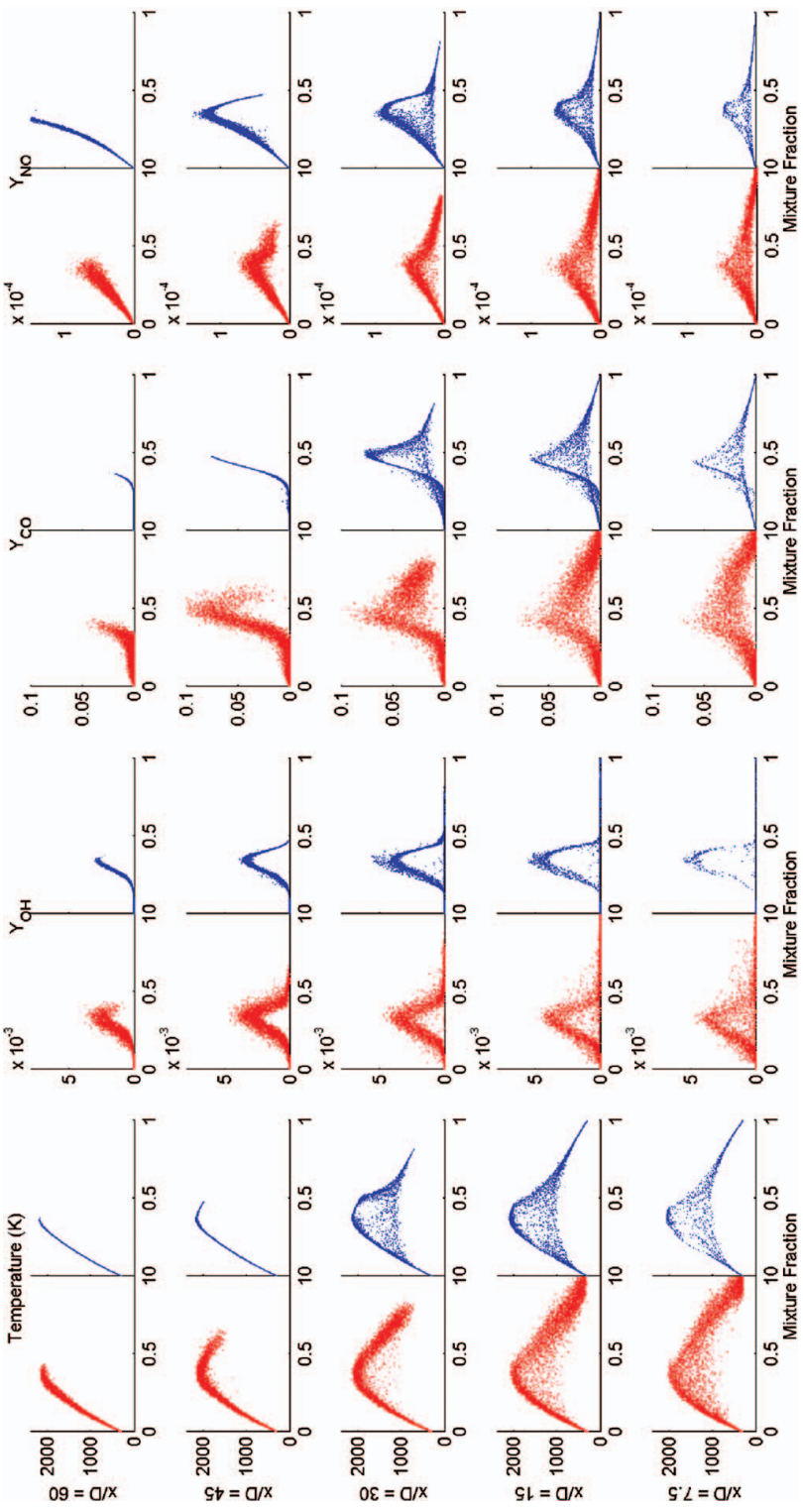

Figure 5. Scatter plots of temperature and mass fractions of CO, NO, and OH plotted vs. mixture fraction at x/D = 7.5, 15, 30, 45, and 60 for flame E. Experiment (Left column); Simulation (Right column).

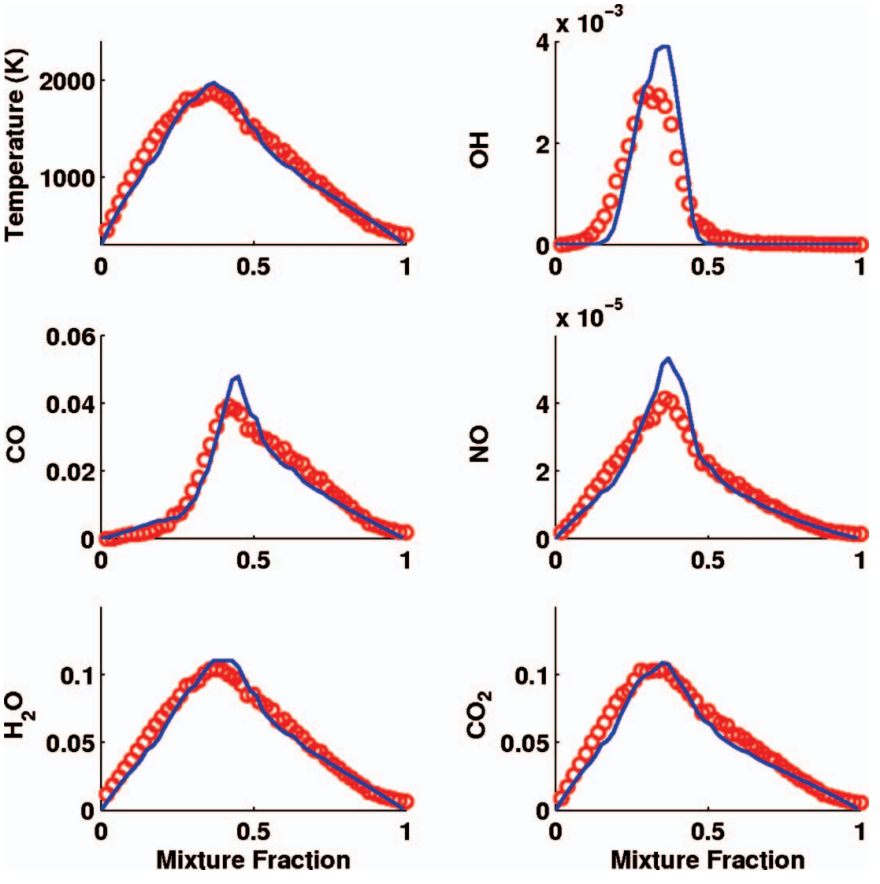

Figure 6. Conditional temperature and mass fractions of CO, H_2O, OH, NO, and CO_2 for flame E at $x/D = 15$; Experiment (circles); Simulation (solid lines).

3.3.1. *'Series E' flames*

Scatter plots for temperature and the mass fractions of OH, CO, CO_2, and NO are shown in Figures 8 and 9 vs. mixture fraction at x/D = 15 and 30 in 'Series E' flames. This is a testing region of these flames where re-ignition is occurring while still showing a significant degree of locally extinguished samples. As the level of oxygen in the 'reconstituted air' increases from 15 to 25% (equiv. to 12 to 18% O_2 by volume in the fuel mixture), the temperature increases as expected and this is seen in the scatter plots of Figures 8 and 9, where a peak temperature of around 2060, 2130, and 2200 K is calculated at $\xi_s = 0.351$ for flames E15, E, and E25, respectively. Also noted in these scatter plots is the broadening in the profiles of OH which reflects the expected broadening in the reaction zones from flames E15 to E25 where $\Delta\xi_R = 0.588$. The more interesting observation here is the increase in the calculated peak mass fractions of OH, CO, and NO with increasing oxygen content as shown on the conditional means in Figures 10 and 11. Peak mass fractions of OH occur at stoichiometric conditions for all flames and increase from 0.0046 in flame E15 to 0.0065 in flame E25. For CO the peak mass fraction increases with oxygenation and shifts further to the rich side. For flame E15 at x/D = 15, peak $Y_{CO} = 0.045$ and close to stoichiometric conditions at $\xi = 0.342$. At x/D = 30, the peak increases to $Y_{CO} = 0.064$ and occurs on the rich side at

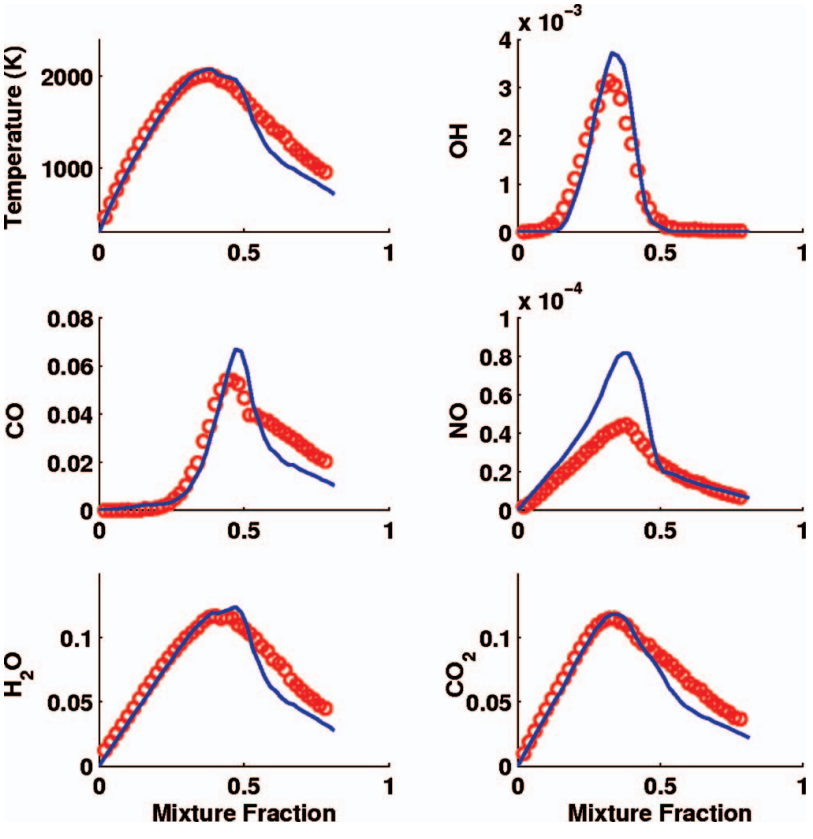

Figure 7. Conditional temperature and mass fractions of CO, H_2O, OH, NO, and CO_2 for flame E at $x/D = 30$; Experiment (circles); Simulation (solid lines).

$\xi = 0.455$ while for flame E25, $Y_{CO} = 0.09$ at $\xi = 0.545$. Peak mass fractions of NO occur around $\xi = 0.36$ for all flames and peak Y_{NO} doubles from flame E15 to flame E25.

The increase in NO with oxygenation is largely due to thermal NO_x imposed by the higher flame temperatures. This is consistent with the laminar flame calculations presented earlier which also show a shift in the peak mass fraction of NO to higher mixture fractions as the level of oxygen increases (flames E15 to E25). The increase in the mass fraction of CO with oxygenation is also consistent with the laminar flames calculations and peak in the mass fraction of CO also shifts to higher mixture fractions. These finding are further supported by plots of conditional means of temperature, OH, NO, CO, CO_2, and H_2O as presented in Figures 10 and 11 for flames in Series E at x/D = 15 and 30, respectively. Throughout the flames, the increase in peak CO and NO mass fractions is markedly higher than that of CO_2.

3.3.2. *'Series B' flames*

Scatter plots for the instantaneous temperature measurements reported earlier for flame B [25,35] are reproduced in Figure 12 to illustrate that moderate local extinction occurs at x/D = 10 while significant local extinction is observed at x/D = 20–30 followed by

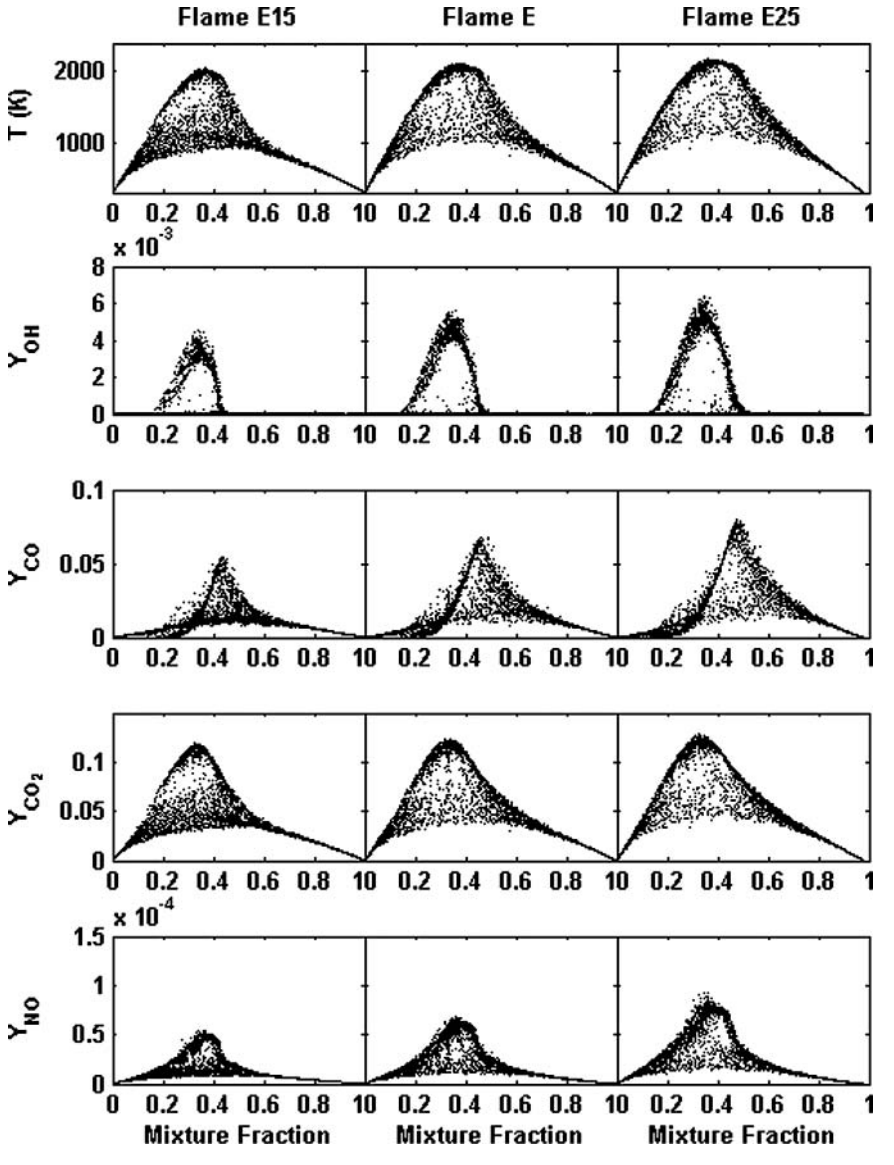

Figure 8. Scatter plots of temperature and the mass fractions of OH, CO, CO_2, and NO plotted vs. mixture fraction for 'Series E' flames from PDF/EMST calculations at x/D = 15.

re-ignition further downstream. The balance of extinction/re-ignition is critical for the overall flame stability but the dynamics of these processes is very sensitive at these intermediate stages of the flame's approach to global blow-off and hence extremely hard to reproduce.

Figure 13 shows a sequence of scatter plots of temperature vs. mixture fraction from the numerical simulation, for various axial locations in flames B, B15, B20, and B25 where the respective reaction zone width increases from $\Delta\xi_R = 0.108$, 0.19, 0.238 to 0.318. Calculations for flames B and B15 show what appears to be local extinction at x/D = 15 and 30 without re-ignition occurring even as far downstream as x/D = 90 which is close to

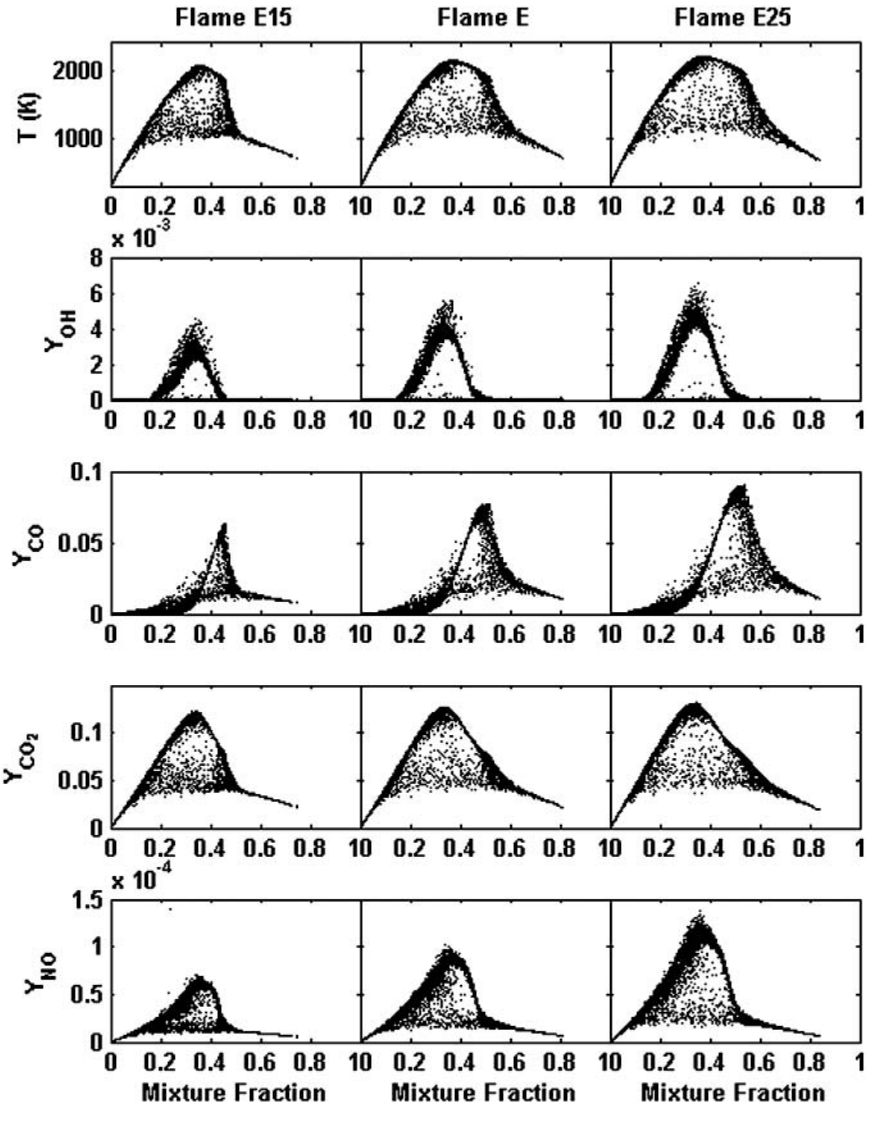

Figure 9. Scatter plots of temperature and the mass fractions of OH, CO, CO_2, and NO plotted vs. mixture fraction for 'Series E' flames from PDF/EMST calculations at x/D = 30.

the tip of the flame. Flame B20 starts to show a pattern closer to expectation where local extinction persists down to x/D = 60 but almost full re-ignition occurs by x/D = 90. Flame B25 shows the most comparable results to the experimental measurements presented in Figure 12, with both extinction and re-ignition correctly captured. The possible problems associated with simulating the flames in 'Series B' using the PDF/EMST approach are discussed below.

3.4. *Limitations of the PDF/EMST approach*

The mixing model used is a pair-wise exchange model based on Euclidean minimum spanning trees (EMST) constructed in composition space and most importantly, accounts

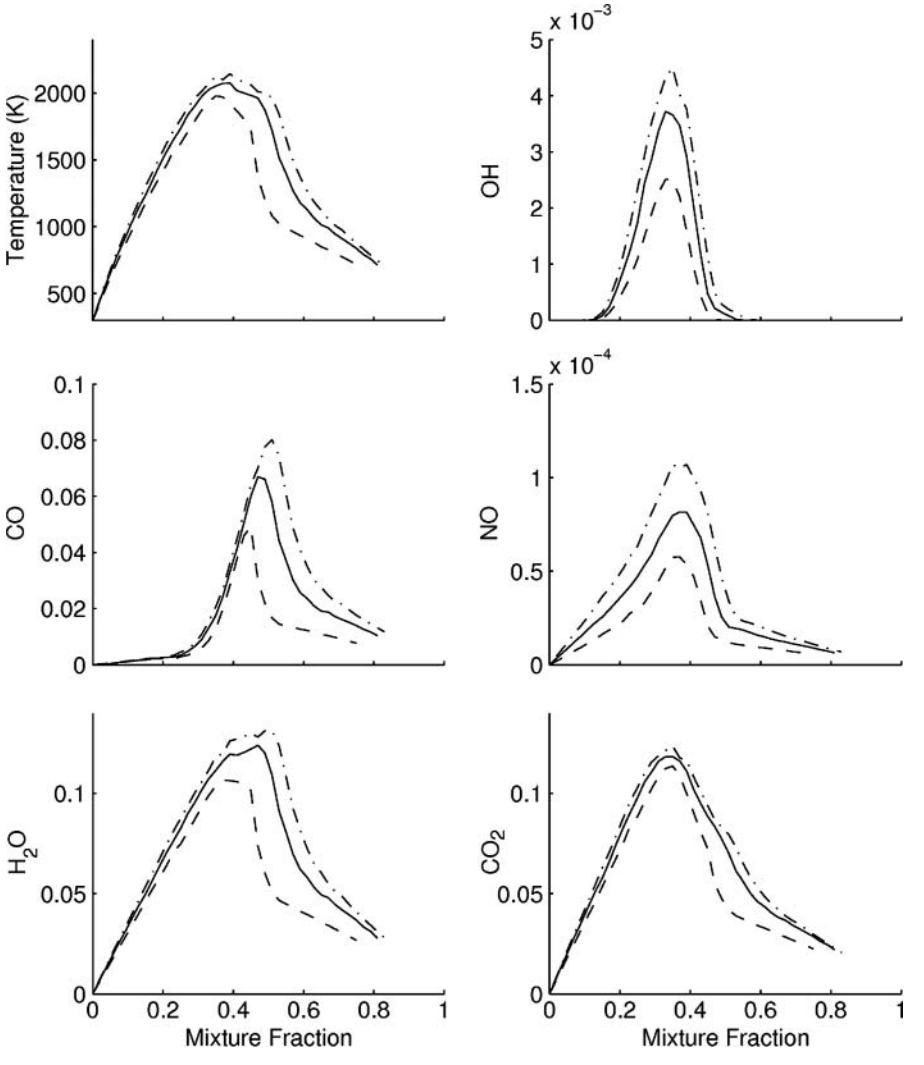

Figure 10. Conditional means of temperature and the mass fractions of OH, CO, CO_2, H_2O, and NO plotted vs. mixture fraction for 'Series E' flames from PDF/EMST calculations at x/D = 15. Flame E15 (dashed line); Flame E (solid line); Flame E25 (dash dot).

for the localness in that composition space. To correctly mimic the behaviour of diffusion flames, mixing models must be local in composition space meaning that particles should be mixing with other particles in their immediate neighbourhood in composition space. Particle interaction models such as Curl's [36] and its variant, the interaction by exchange with the mean (IEM) [37], also known as linear mean square estimation (LMSE) [38] approach, are not local in composition space but in physical space instead. The EMST mixing model accounts for this localness in composition space and has been proven to be an excellent model to simulate diffusion flames [31,39–41]. On the other hand, the model shows some limitations when dealing with turbulent diffusion flames with narrow reactions zones in mixture fraction space, as discussed next.

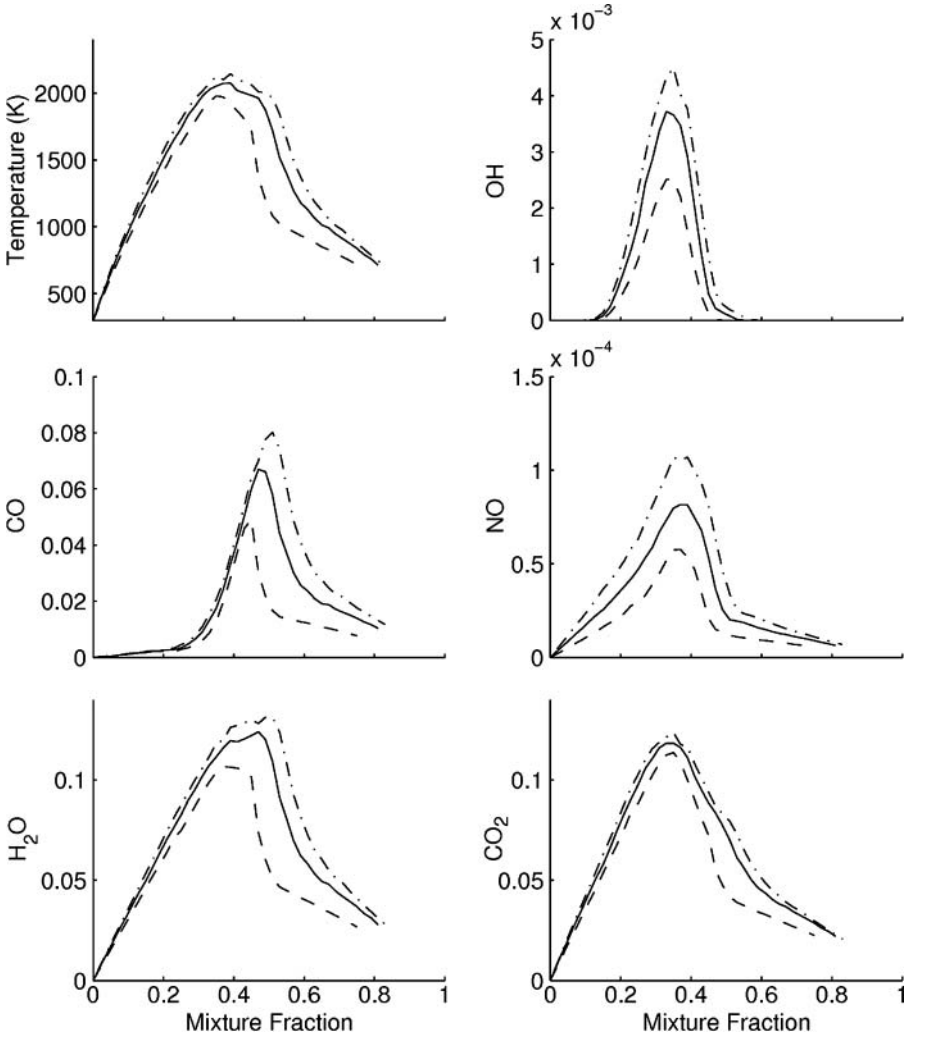

Figure 11. Conditional means of temperature and the mass fractions of OH, CO, CO_2, H_2O, and NO plotted vs. mixture fraction for 'Series E' flames from PDF/EMST calculations at x/D = 30. Flame E15 (dashed line); Flame E (solid line); Flame E25 (dash dot).

It is evident from Figure 13 that what appears to be local extinction is more like significant 'stranding' imposed by the EMST mixing process, pulling particles to a lower asymptote that corresponds to mixtures that are partially burnt or simply mixed with hot combustion products. This 'stranding' phenomenon was identified by Subramaniam and Pope [30] in the early analysis of the mixing model, and an intermittency feature to alleviate this deficiency was introduced. The feature, which is independent of the number of particle per cell and the number of scalars, operates on the basis that particles are set to either be in a mixing state, where their composition changes due to mixing, or a non-mixing state where a particle's composition remains unchanged due to mixing. A non-dimensional property is associated with each particle to determine the mixing timescale. The time a particle spends in either the mixing or non-mixing states is also scaled with the turbulence

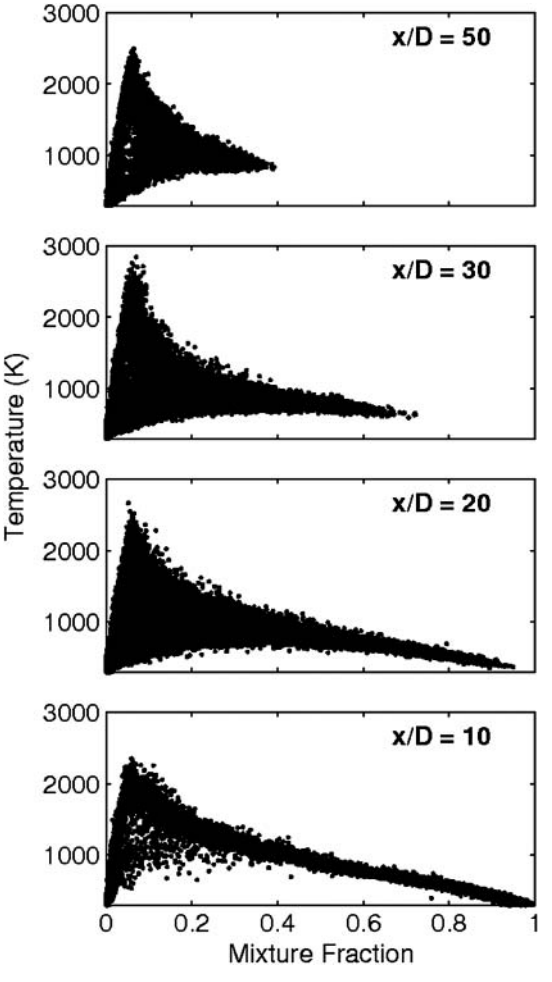

Figure 12. Scatter plots of temperature (K) plotted vs. mixture fraction for flame B from experimental results, at x/D = 10, 20, 30, and 50.

timescale (κ–ε), and the EMST model approach operates based on only particles that are in the mixing state in composition space, during that time [30]. Fuels with low stoichiometric mixture fractions may have narrow reaction zones in composition space, where numerically, only a small amount of particles are undergoing molecular mixing followed by reaction while the rest are undergoing a non-reactive mixing process (mixing with no change in composition). The effect is that there are fewer reactive particles to pull the non-mixing particles up to their reactive regime, thus the numerical solution fails to capture the re-ignition process and maintain a stable burning flame. Increasing the C_{φ} value would decrease the simulated amount of local extinction [31] and although may help improving the calculations of these flames, will still be an artificial way of capturing the real dynamics of the re-ignition processes. It must also be noted that the age process model constants have been determined with no direct support from physical evidence but to enhance the mixing model performance [30]. Alterations to these model constants may also help alleviate the 'stranding' phenomenon further and can be the subject of future investigations.

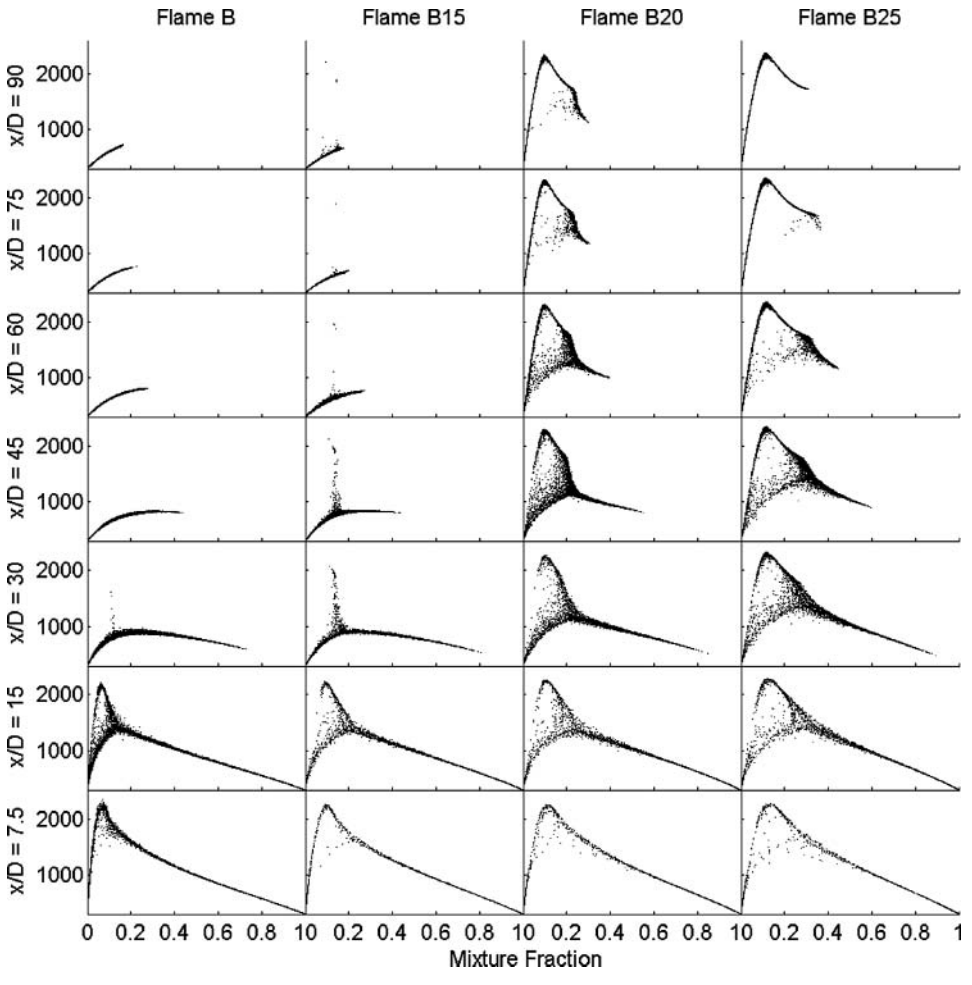

Figure 13. Scatter plots of temperature (K) plotted vs. mixture fraction for 'Series B' flames from PDF/EMST calculations, at x/D = 7.5, 15, 30, 45, 60, 75, and 90.

As the reaction zone width increases with oxygenation, flame B20 starts to show a pattern closer to expectation where local extinction persists with only some 'stranding' down to x/D = 60 but almost full re-ignition occurs by x/D = 90. Both extinction and re-ignition is captured in flame B25, which shows the most comparable results to the experimental measurements presented in Figure 12, albeit with some minor 'stranding' remaining at a mixture fraction of between $\xi_s = 0.3$–0.4. It seems that the reaction zone width in mixture fraction space needs to be at $\Delta\xi_R = 0.25$ or higher for the PDF/EMST approach to capture adequately the extinction and re-ignition characteristics of flames approaching global blow-off. Flames in 'Series E' have reaction zone widths varying from $\Delta\xi_R = 0.4$ to 0.59, all of which are above the calculated minimum of 0.25, and therefore the PDF/EMST approach successfully simulates these flames.

It is evident that the EMST mixing model has shown some limitations and more advanced models are needed to enable the PDF approach to capture the transient features of flames with thinner reaction zones. It should be pointed out however, that the difficulty

in computing flames with thin reaction zones is not limited to the PDF/EMST approach. Methane flames L, B, M have been measured experimentally since the eighties and, as yet, the latter two are not reproduced numerically either by flamelet models or by conditional moment closure (CMC) methods. The difficulty here arises in the fluctuations in the scalar dissipation rates and the different transients associated with the extinction and re-ignition processes. The advent of high-speed LIF imaging is beginning to shed light on these issues with respect to the rate of occurrence of these transient events [42–44]. Such time transients involve not only local extinction events but also flames 'closures' which occur as the local scalar dissipated rates are relaxed. It appears that edge flames play key roles in such occurrences. Large eddy simulations coupled with a suitable sub-grid scale model for combustion (either a filtered density function or linear eddy model) may well be able to reproduce such intricacies. MMC methods [4,45] are also showing promising results in this regard.

4. Conclusions

The stability limits of the range of piloted turbulent partially-premixed flames of CNG investigated increase almost linearly with the amount of oxygen in the fuel–O_2–N_2 mixture and also with the pilot heat release rate. PDF calculations that use detailed chemistry and the EMST mixing model, fail to reproduce the finite-rate chemistry effects in flames such as pure CNG flames. This is thought to be due to the limitation of the EMST approach to correctly simulate turbulent flames with narrow reaction zones and approaching extinction. The model fails to capture the correct patterns of mixing in these flames but when the fuel is sufficiently diluted with oxygen, so that the reaction zone width in mixture fraction space is greater than around 0.25, a significant improvement in the PDF calculations is observed, as shown for flame B25 and all flames in 'Series E'. The higher levels of oxygen also produce an increase in CO and NO levels due to the higher flame temperatures, and this is consistent with laminar flame calculations as well as with the experimental findings.

Acknowledgments

This research is supported by the Australian Research Council. Prof. S.B. Pope's contribution was supported by Air Force Office of Scientific Research under Grant FA-9550-09-1-0047.

References

[1] S.B. Pope, Progress Energy Combust. Sci. *11* (2) (1985), pp. 119–192.
[2] A.Y. Klimenko, and R.W. Bilger, Progress Energy Combust. Sci. *25* (6) (1999), pp. 595–687.
[3] R.W. Bilger, Phys. Fluids A: Fluid Dyn. *5* (2) (1993), pp. 436–444.
[4] M. Cleary, and A. Klimenko, Flow Turbul. Combust. *82* (4) (2009), pp. 477–491 DOI: 10.1007/s10494–008-9161–3.
[5] N. Peters, Symp. (Int.) Combust. *20* (1) (1985), pp. 353–360.
[6] N. Peters, Progress Energy Combust. Sci. *10* (3) (1984), pp. 319–339.
[7] E. Knudsen, and H. Pitsch, Combust. Flame *156* (3) (2009), pp. 678–696.
[8] M. Ihme, and H. Pitsch, Combust. Flame *155* (1–2) (2008), pp. 90–107.
[9] C.D. Pierce, and P. Moin, J. Fluid Mech. *504* (1) (2004), pp. 73–97.
[10] R.W. Grout, N. Swaminathan, and R.S. Cant, Combust. Theor. Model. *13* (5) (2009), pp. 823–852.
[11] C. Duwig, and C. Fureby, Combust. Flame *151* (1–2) (2007), pp. 85–103.
[12] B. Fiorina, O. Gicquel, L. Vervisch, S. Carpentier, and N. Darabiha, Combust. Flame *140* (3) (2005), pp. 147–160.

[13] M.J. Dunn, A.R. Masri, R.W. Bilger, R.S. Barlow, and G.H. Wang, Proc. Combust. Inst. *32* (2) (2009), pp. 1779–1786.
[14] F. Seffrin, F. Fuest, D. Geyer, and A. Dreizler, Combust. Flame *157* (2) (2010), pp. 384–396.
[15] P. Anselmo-Filho, S. Hochgreb, R.S. Barlow, and R.S. Cant, Proc. Combust. Inst. *32* (2) (2009), pp. 1763–1770.
[16] J.E. Dec, Proc. Combust. Inst. *32* (2) (2009), pp. 2727–2742.
[17] M. Sjöberg, and J.E. Dec, Proc. Combust. Inst. *30* (2) (2005), pp. 2719–2726.
[18] R.S. Barlow, and J.H. Frank, Symp. (Int.) Combust. *27* (1) (1998), pp. 1087–1095.
[19] Z. Cheng, J.A. Wehrmeyer, and R.W. Pitz, Combust. Sci. Technol. *178* (12) (2006), pp. 2145–2163.
[20] T.F. Wall, Proc. Combust. Inst. *31* (1) (2007), pp. 31–47.
[21] B.J.P. Buhre, L.K. Elliott, C.D. Sheng, R.P. Gupta, and T.F. Wall, Progress Energy Combust. Sci. *31* (4) (2005), pp. 283–307.
[22] A.R. Masri, and R.W. Bilger, Symp. (Int.) Combust. *21* (1) (1988), pp. 1511–1520.
[23] A.N. Karpetis, and R.S. Barlow, Proc. Combust. Inst. *30* (1) (2005), pp. 665–672.
[24] M.G. Zabetakis, Bulletin 627, U.S. Department of the Interior, Bureau of Minus, 1965.
[25] A.R. Masri, R.W. Dibble, and R.S. Barlow, Progress Energy Combust. Sci. *22* (4) (1996), pp. 307–362.
[26] CANTERA An Object-Oriented Software package for Reacting Flows, Release 1.6.0. http://www.cantera.org.
[27] C.J. Sung, C.K. Law, and J.Y. Chen, Combust. Flame *125* (1–2) (2001), pp. 906–919.
[28] S.B. Pope, Combust. Theor. Model. *1* (1) (1997), pp. 41–63.
[29] B.J.D. Liu, and S.B. Pope, Combust. Theor. Model. *9* (4) (2005), pp. 549–568.
[30] S. Subramaniam, and S.B. Pope, Combust. Flame *115* (4) (1998), pp. 487–514.
[31] J. Xu, and S.B. Pope, Combust. Flame *123* (3) (2000), pp. 281–307.
[32] TNF International Workshop on Measurement and Computation of Turbulent (Non)Premixed Flames. Available at http://www.sandia.gov/TNF/.
[33] C.T. Bowman, R.K. Hanson, D.F. Davidson, J.W.C.Gardiner, V. Lissianski, G.P. Smith, D.M. Golden, M. Frenklach, and M. Goldenberg GRI-MECH 2.11. Available at http://www.me.berkeley.edu/gri_mech/.
[34] R.R. Cao, and S.B. Pope, Combust. Flame *143* (4) (2005), pp. 450–470.
[35] Sydney Piloted Flame Database. Available at http://sydney.edu.au/engineering/aeromech/thermofluids/piloted_files/data/pf01.zip.
[36] R.L. Curl, Am. Inst. Chem. Eng. *9* (2) (1963), pp. 175–181.
[37] J. Villermaux, and J.C. Devillon, Int. Symp. Chem. React. Eng. *2* (1972), pp. B1.
[38] C. Dopazo, Phys. Fluids *18* (4) (1975), pp. 397–404.
[39] R.R. Cao, S.B. Pope, and A.R. Masri, Combust. Flame *142* (4) (2005), pp. 438–453.
[40] H. Wang, and Y. Chen, Chem. Eng. Sci. *59* (16) (2004), pp. 3477–3490.
[41] Q. Tang, J. Xu, and S.B. Pope, Proc. Combust. Inst. *28* (1) (2000), pp. 133–139.
[42] B. Böhm, C. Heeger, I. Boxx, W. Meier, and A. Dreizler, Proc. Combust. Inst. *32* (2) (2009), pp. 1647–1654.
[43] I. Boxx, C. Heeger, R. Gordon, B. Böhm, M. Aigner, A. Dreizler, and W. Meier, Proc. Combust. Inst. *32* (1) (2009), pp. 905–912.
[44] C. Kittler, and A. Dreizler, Appl. Phys. B: Lasers Optics *89* (2) (2007), pp. 163–166.
[45] Y. Ge, M.J. Cleary, and A.Y. Klimenko, Proc. Combust. Inst. *33* (1) (2011), pp. 1401–1409.